FROM BROAD EXPLORATION TO STABLE SYNTHESIS: ENTROPY-GUIDED OPTIMIZATION FOR AUTOREGRES-SIVE IMAGE GENERATION

Anonymous authors

Paper under double-blind review

ABSTRACT

Combining Chain-of-Thought (CoT) with Reinforcement Learning (RL) improves text-to-image (T2I) generation, yet the underlying interaction between CoT's exploration and RL's optimization remains unclear. We present a systematic entropy-based analysis that yields three key insights: (1) CoT expands the generative exploration space, while RL contracts it toward high-reward regions; (2) final reward is strongly negatively correlated with both the mean and variance of image-token entropy, highlighting the need to reduce uncertainty and instability; and (3) the entropy of the textual CoT directly governs downstream image quality, with lower-entropy CoTs leading to better generations. Motivated by these findings, we propose *Entropy-Guided Group Relative Policy Optimization* (EG-GRPO), a fine-tuning strategy that reallocates optimization budget by uncertainty: low-entropy tokens are excluded from reward-driven updates to preserve stability, while highentropy tokens receive an entropy bonus that encourages structured exploration without collapse. Experiments on standard T2I benchmarks demonstrate that EG-GRPO achieves state-of-the-art performance.

1 Introduction

Text-to-image (T2I) generation has progressed rapidly with large-scale pretraining and strong autoregressive and diffusion architectures (Chen et al., 2023; Labs, 2024; Wang et al., 2024), yet two core challenges remain: (i) balancing *exploration* for diversity against *exploitation* for reward-aligned fidelity, and (ii) ensuring *generation stability* under repeated sampling. Chain-of-Thought (CoT) prompting promises richer semantic planning (Wei et al., 2022), while reinforcement learning (RL) directly optimizes task or preference rewards (Jiang et al., 2025). However, how CoT's exploratory behavior interacts with RL's optimization in T2I, and how this interaction governs uncertainty and stability, has not been systematically understood.

We analyze *entropy dynamics* in autoregressive T2I models that combine CoT with RL (via Group Relative Policy Optimization, GRPO (Jiang et al., 2025)) and use Shannon entropy to quantify token-level uncertainty in both modalities: textual CoT tokens and image tokens. Three empirical findings emerge. First, CoT *expands* the exploration space, broadening the entropy distribution of generated outputs, whereas RL *contracts* this space toward higher-reward regions. Second, final reward exhibits a strong negative correlation with both the *mean* and the *standard deviation* of image-token entropy, indicating that reducing uncertainty and instability is central to quality. Third, the entropy of the textual CoT *directly* influences downstream image quality: lower-entropy CoTs yield tighter, higher-reward clusters under stable sampling.

Guided by these findings, we propose *Entropy-Guided Group Relative Policy Optimization (EG-GRPO)*, a token-level modification of GRPO that reallocates gradient budget by uncertainty. Lowentropy (high-confidence) tokens are excluded from reward-driven updates, retaining only the KL-to-reference term to preserve stability and previously acquired knowledge. High-entropy tokens receive an *entropy bonus* added to the advantage, encouraging structured exploration and accelerating uncertainty reduction where it matters. A batch-level calibration ties the bonus magnitude to the mass saved on low-entropy tokens, keeping update scale close to GRPO, and the bonus vanishes at GRPO equilibrium, preserving the stationary points of the base objective (Wang et al., 2025b).

We evaluate EG-GRPO on T2I-CompBench (Huang et al., 2023) and WISE (Niu et al., 2025) using a Janus-Pro autoregressive backbone in a discrete latent space (Chen et al., 2025) and a standard reward pipeline combining human-preference scoring, object grounding, and VQA signals (Wu et al., 2023; Liu et al., 2024; Wang et al., 2022). EG-GRPO attains state-of-the-art results, with pronounced gains in compositional generalization (e.g., attribute binding and object relations). Ablations that apply entropy guidance to only CoT tokens or only image tokens underperform the full model, confirming the need to control uncertainty in both semantic planning and visual decoding.

The main contributions of our paper can be summarized as follows:

- We provide a quantitative account of the CoT–RL interaction through entropy dynamics: CoT expands exploration, RL contracts toward high-reward regions; reward is strongly negatively correlated with entropy mean and std; and textual CoT entropy governs downstream image quality.
- We introduce an entropy-guided, token-level refinement of GRPO that protects confident tokens via KL-only updates and focuses optimization on uncertain tokens via an entropy bonus, with calibrated budget and equilibrium-vanishing properties.
- On T2I-CompBench and WISE, EG-GRPO achieves state-of-the-art performance and reduces uncertainty and instability in line with the analysis.

2 RELATED WORK

2.1 Text-to-Image generation Model

Text-to-image generation has been advanced along two major paradigms: autoregressive modeling and diffusion-based approaches. On the autoregressive side, Parti Yu et al. (2022) demonstrates that large-scale transformer models can achieve impressive compositional generation by predicting image tokens sequentially. Fluid Fan et al. (2024) further explores continuous tokens and generation order, showing improved efficiency and quality. STAR Ma et al. (2024) introduces a scale-wise autoregressive framework that progressively generates images from coarse to fine scales, while Jet-Former Tschannen et al. (2024) directly models raw images and text in a unified autoregressive manner without discrete tokenization. More recently, NextStep-1 Team et al. (2025) scales continuoustoken autoregressive generation to 14B parameters, achieving strong performance in both image synthesis and editing. In parallel, diffusion models have become dominant for high-quality synthesis. VO-Diffusion Gu et al. (2022) combines vector-quantized representations with diffusion for discrete latent modeling, and ERNIE-ViLG 2.0 Feng et al. (2023) extends this to large-scale multilingual text-to-image generation. UPainting Li et al. (2022) introduces cross-modal guidance to unify simple and complex scenarios, while RPG Yang et al. (2024) enhances controllability via recaptioning, planning, and region-based diffusion. These works illustrate the complementary strengths of autoregressive and diffusion frameworks in advancing the controllability, fidelity, and scalability of text-to-image generation.

2.2 Chain of Thinking and Reinforcement Learning

Recent works have explored integrating Chain-of-Thought (CoT) reasoning with reinforcement learning (RL) to improve text-to-image generation. Visual-CoG Li et al. (2025) introduces stage-aware RL with intermediate rewards across semantic planning, refinement, and evaluation, while ReasonGen-R1 Zhang et al. (2025b) and T2I-R1 Jiang et al. (2025) incorporate rationale-augmented data and bi-level reasoning chains optimized via GRPO. PromptEnhancer Wang et al. (2025a) further demonstrates that CoT-based prompt rewriting with RL can enhance image quality without modifying the generator, and verification-based methods also inject preference alignment during synthesis Zhang et al. (2025a). Beyond explicit CoT, RL has been applied for alignment in diffusion models, such as comparing DPO and GRPO Tong et al. (2025), subject-driven preference optimization Miao et al. (2024), and DPOK fine-tuning with KL regularization Fan et al. (2023). Related multimodal reasoning approaches, including ImageGen-CoT Liao et al. (2025) and reflective CoT for retrieval Wu et al. (2024), highlight the broader potential of structured reasoning. Combining CoT and RL provides a promising avenue for enhancing controllability, interpretability, and human alignment in text-to-image generation.

3 Preliminaries

We begin by formalizing autoregressive text-to-image generation, introducing Shannon entropy as a measure of generative uncertainty, and reviewing Group Relative Policy Optimization (GRPO) for model refinement.

3.1 AUTOREGRESSIVE GENERATION IN DISCRETE LATENT SPACE

Autoregressive text-to-image models operate in a discrete latent space. An image I is first encoded into tokens $z=(z_1,z_2,\ldots,z_L)$ via a pre-trained tokenizer such as VQ-VAE. The conditional likelihood given a text prompt c factorizes autoregressively:

$$p(z \mid c) = \prod_{i=1}^{L} p(z_i \mid z_{< i}, c).$$
 (1)

A policy π_{θ} parameterized by θ models these conditionals. At step i, the policy outputs a categorical distribution $\pi_{\theta}(\cdot \mid z_{< i}, c)$ over the vocabulary \mathcal{V} , from which z_i is sampled. The final image is reconstructed by decoding the full sequence z.

3.2 Entropy as Predictive Uncertainty

For each step i, the policy distribution admits a Shannon entropy:

$$H(\pi_{\theta}(\cdot \mid z_{< i}, c)) = -\sum_{j \in \mathcal{V}} p_j \log p_j, \tag{2}$$

where p_j denotes the probability of token j. Low entropy reflects confident, often high-fidelity predictions with reduced diversity, whereas high entropy reflects uncertainty, encouraging exploration and diverse generations at the cost of possible incoherence.

3.3 GROUP RELATIVE POLICY OPTIMIZATION

Group Relative Policy Optimization (GRPO) refines generative policies using relative rewards without requiring a value function. For a prompt c, the policy π_{θ} samples G candidate sequences

$$\{o^{(i)}\}_{i=1}^G \sim \pi_{\theta}(\cdot \mid c), \quad o^{(i)} = (o_1^{(i)}, \dots, o_{T^{(i)}}^{(i)}).$$
 (3)

Each sequence receives a reward $r^{(i)}$, which is normalized within the group:

$$\mu = \frac{1}{G} \sum_{i=1}^{G} r^{(i)}, \quad \sigma = \sqrt{\frac{1}{G} \sum_{i=1}^{G} (r^{(i)} - \mu)^2}, \quad A^{(i)} = \frac{r^{(i)} - \mu}{\max\{\sigma, \varepsilon\}}.$$
 (4)

Broadcasting $A^{(i)}$ to all tokens yields the training objective

$$\mathcal{L}_{GRPO}(\theta) = -\frac{1}{G} \sum_{i=1}^{G} \frac{1}{T^{(i)}} \sum_{t=1}^{T^{(i)}} A^{(i)} \log \pi_{\theta}(o_{t}^{(i)} \mid c, o_{< t}^{(i)}) + \beta D_{KL}(\pi_{\theta} \parallel \pi_{ref}), \tag{5}$$

where $\beta \geq 0$ controls a KL regularizer toward a reference policy. This group-based normalization yields scale-invariant advantages and stable updates, making GRPO well-suited for aligning autoregressive generators with task-specific rewards.

4 Analysis of Entropy Dynamics in Text-to-Image Generation

To investigate the role of uncertainty in text-to-image generation, we analyze *generative entropy* as a quantitative indicator of model behavior. Our study focuses on disentangling how CoT and RL fine-tuning affect entropy within the pipeline. By examining their individual and combined effects, we clarify how these techniques balance exploration and exploitation, and how the resulting entropy dynamics define the optimization objective for high-quality visual synthesis.

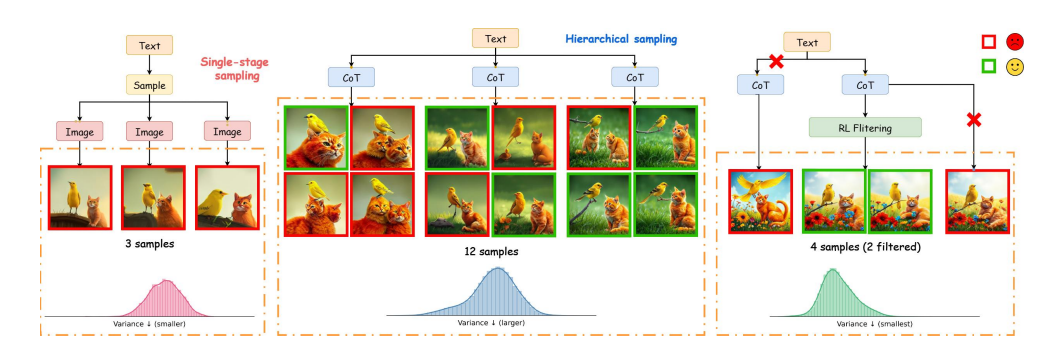


Figure 1: Comparison of different text-to-image generation methods: (a) autoregressive text-to-image generation, (b) CoT, and (c) with CoT and GRPO optimization.

4.1 THE DICHOTOMY OF EXPLORATION AND EXPLOITATION: COT vs. RL

We begin our analysis by examining the distinct yet complementary roles of Chain-of-Thought (CoT) prompting and reinforcement learning (RL) fine-tuning. For each textual prompt, we generate multiple image candidates under three settings: the baseline model (Janus-Pro), the baseline augmented with CoT reasoning (Janus-Pro+CoT), and a GRPO-finetuned variant built upon Janus-Pro+CoT (T2I-RI). To investigate their differences, we assess each generated image by jointly measuring its output mean entropy and reward score, and visualize the resulting distributions in a two-dimensional space.

As illustrated in Figure 2, the introduction of CoT significantly broadens the entropy distribution of the generated images. It shows that CoT expands the model's exploratory space, enabling it to generate a more diverse set of outputs. This expanded space contains both low- and high-reward samples, indicating that CoT itself does not guarantee quality but rather increases the range of generative possibilities. Conversely, the application of Group Relative Policy Optimization (GRPO), which results in the T2I-R1, leads to a notable contraction and leftward shift of the entropy distribution. This demonstrates that the model learns to exploit the vast space unlocked by CoT, converging towards a much narrower, lower-entropy region that consistently yields higher rewards. This reveals a complementary relationship: CoT serves to expand the exploratory landscape, while RL acts as a refinement mechanism to exploit this landscape and guide the model towards stable, high-quality regions.

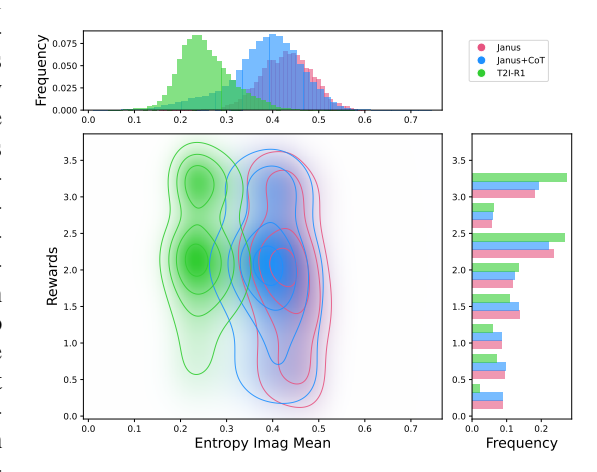


Figure 2: Entropy–reward distributions of different methods. CoT (*Janus-Pro+CoT*) expands the exploratory space with more diverse outputs, while GRPO fine-tuning (*T2I-RI*) contracts it toward higher-reward regions, yielding more stabilized, high-quality generations.

4.2 Upstream Influence: How Cot's Textual Entropy Governs Image Quality

Since Chain-of-Thought serves as the entry point of exploration, we further examine how the intrinsic uncertainty of the textual CoT affects downstream image generation. To isolate this effect, we focus on a subset of samples where image generation remains stable, defined as those with entropy variance below a small threshold of 0.011 across multiple runs. This filtering minimizes confounding factors due to unstable sampling, allowing us to probe the impact of CoT entropy directly.

As shown in Figure 3 (Left), we observe a clear negative correlation between the mean entropy of the textual CoT and the average reward of the resulting images. Intuitively, high-entropy CoTs correspond to less coherent or more uncertain reasoning traces, which tend to degrade visual quality.

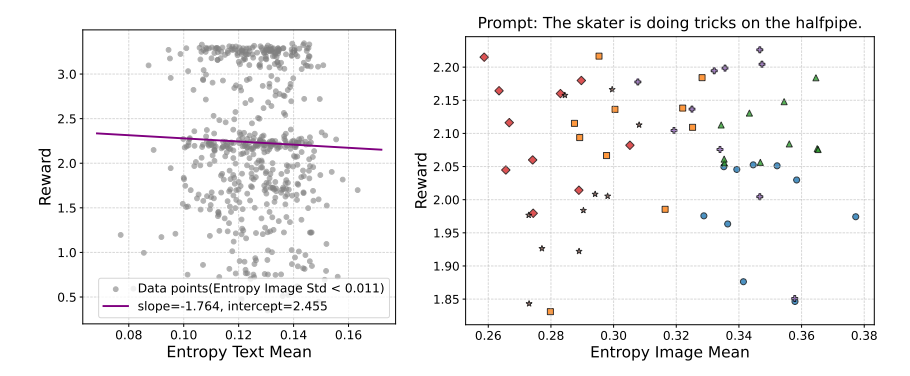


Figure 3: **Left:** Reward vs. CoT entropy (stable cases, Image Entropy Std < 0.011). Higher CoT entropy correlates with lower image reward. **Right:** Reward distributions across different CoTs for the same prompt. Images from the same CoT cluster together, with certain CoTs consistently yielding lower rewards.

In contrast, low-entropy CoTs provide more confident and consistent reasoning, ultimately leading to higher-reward generations. This analysis is grounded on the stable subset, ensuring that the observed trend is not an artifact of sampling instability.

To further dissect this phenomenon, we visualize the reward distributions of images conditioned on different CoTs for the same prompt (Figure 3, Right). Each distinct CoT forms a compact cluster in the reward space, highlighting its consistent influence on generation outcomes. Notably, certain CoTs repeatedly produce clusters with lower average rewards, suggesting that the quality bottleneck is determined upstream, at the textual reasoning stage. These findings demonstrate a direct transmission of uncertainty from text to image: the entropy of CoT reasoning acts as a critical upstream factor that governs the attainable quality of visual outputs.

4.3 THE LEARNED OBJECTIVE: MINIMIZING UNCERTAINTY AND INSTABILITY FOR HIGHER REWARDS

We next investigate how the fully RL-trained model internalizes entropy control to optimize for reward. For each prompt–CoT pair, multiple images are generated, and their entropy statistics are aggregated. Specifically, the mean entropy characterizes the global level of uncertainty in the generative process, while the standard deviation (std) captures the degree of instability across different runs.

Empirical results reveal a consistent negative correlation between reward and standard deviation of entropy (Figure 4, Left). This indicates that generative instability is inherently detrimental: mod-

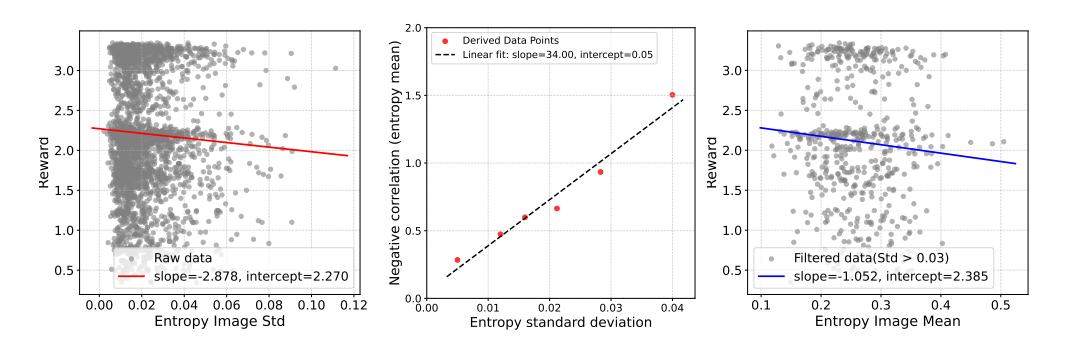


Figure 4: **Left:** Reward vs. entropy std. Higher instability (larger std) consistently lowers reward. **Middle:** Relation between entropy std (x-axis) and the negative correlation of reward–entropy mean (y-axis). Greater instability strengthens the negative correlation. **Right:** Reward vs. entropy mean under high-variance cases (std > 0.03). Large std implies exploratory generation where RL has not converged; in this regime, reducing mean entropy is especially beneficial.

els that produce more consistent entropy trajectories across samples yield higher-quality outputs. Beyond this first-order observation, we further examine how instability modulates the role of uncertainty. Figure 4 (Middle) demonstrates that the negative correlation between mean entropy and reward becomes progressively stronger as std increases. In other words, instability amplifies the adverse impact of uncertainty, rendering mean entropy a more decisive factor under high-variance conditions.

To isolate this effect, we analyze the high-variance regime (std > 0.03), where the image token generation remains exploratory and the RL policy has not yet converged. As shown in Figure 4 (Right), in such cases, lowering mean entropy proves particularly effective in improving reward. This finding suggests that, when the model operates in an unstable exploratory state, suppressing overall uncertainty is a critical pathway toward higher-quality generations.

These analyses indicate that the RL agent implicitly optimizes a compound objective: simultaneously minimizing overall uncertainty (mean entropy) and reducing instability across runs (entropy std).

5 ENTROPY-GUIDED GROUP RELATIVE POLICY OPTIMIZATION

Building on Section 4, we introduce a token-level optimization scheme that preserves GRPO's group-relative structure while reallocating updates toward uncertain parts of the generation process. *Entropy-Guided GRPO (EG-GRPO)* applies to both textual CoT and image tokens and adds an entropy-based bonus only where uncertainty is high.

5.1 DESIGN PRINCIPLES FROM ENTROPY ANALYSIS

Section 4 showed that: (i) CoT broadens exploration while RL contracts it toward high-reward regions; (ii) rewards are negatively correlated with both the mean and the variance of token entropies; and (iii) textual (CoT) entropy causally influences downstream image quality. We adopt three principles:

- Focus on uncertainty. Allocate more update mass to high-entropy tokens to reduce instability where it matters.
- 2. **Protect confidence.** On the lowest-entropy tokens, set the reward-driven advantage to zero so that only the KL-to-reference acts, preventing drift on confident regions.
- 3. **Stay reward-driven.** Retain the GRPO group-relative objective; entropy contributes an *additive* per-token bonus at high entropy without replacing advantage.

5.2 REVISITING GRPO AND TOKEN BROADCAST

For prompt c, policy π_{θ} samples G sequences $\{o^{(i)}\}_{i=1}^{G}$ with rewards $\{r^{(i)}\}$ normalized to group-relative advantages $A^{(i)}$. GRPO optimizes

$$\mathcal{L}_{GRPO}(\theta) = -\frac{1}{G} \sum_{i=1}^{G} \frac{1}{T^{(i)}} \sum_{t=1}^{T^{(i)}} A^{(i)} \log \pi_{\theta} (o_{t}^{(i)} \mid c, o_{< t}^{(i)}) + \beta D_{KL} (\pi_{\theta} \parallel \pi_{ref}).$$
 (6)

This *broadcasts* the same coefficient $A^{(i)}$ to all tokens of sequence i, ignoring per-token uncertainty and potentially wasting gradient budget on already-confident tokens.

5.3 Entropy-Guided Token Selection

Let $H_t^{(i)} \triangleq H(\pi_\theta(\cdot \mid c, o_{< t}^{(i)}))$ be the Shannon entropy at token t of sequence i, and define the normalized entropy $\bar{H}_t^{(i)} \triangleq H_t^{(i)}/\log |\mathcal{V}| \in [0,1]$. For each sequence i and each modality $m \in \{\text{text, image}\}$ independently, l compute per-sequence percentiles and define

$$\mathcal{S}_{\mathrm{hi}}^{(i,m)} = \text{top-}50\% \text{ by } \bar{H}_t^{(i)}, \quad \mathcal{S}_{\mathrm{lo}}^{(i,m)} = \text{bottom-}20\%, \quad \mathcal{S}_{\mathrm{mid}}^{(i,m)} = \text{remaining}.$$

¹We rank and threshold entropies on textual CoT and image tokens separately, consistent with Section 4.

Introduce masks $M_t^{(i)}, U_t^{(i)} \in \{0, 1\}$:

$$M_t^{(i)} = \mathbb{I}[t \notin \mathcal{S}_{\text{lo}}^{(i,m)}], \qquad U_t^{(i)} = \mathbb{I}[t \in \mathcal{S}_{\text{hi}}^{(i,m)}],$$

so $M_t^{(i)}=0$ removes reward-driven updates on low-entropy tokens, and $U_t^{(i)}=1$ marks high-entropy tokens to receive a bonus.

Budget view. Let $p_{\text{lo}}, p_{\text{mid}}, p_{\text{hi}}$ be the fractions of tokens in $\mathcal{S}_{\text{lo}}^{(i,m)}, \mathcal{S}_{\text{mid}}^{(i,m)}, \mathcal{S}_{\text{hi}}^{(i,m)}$ ($p_{\text{hi}} = 0.5$, $p_{\text{lo}} = 0.2, p_{\text{mid}} = 0.3$). GRPO's per-sequence coefficient budget is $B_{\text{GRPO}}^{(i)} \triangleq \frac{1}{T^{(i)}} \sum_{t=1}^{T^{(i)}} |A^{(i)}| = |A^{(i)}|$. Under EG-GRPO,

$$B_{\text{EG}}^{(i)} \triangleq \frac{1}{T^{(i)}} \sum_{t=1}^{T^{(i)}} \left| M_t^{(i)} A^{(i)} + U_t^{(i)} \lambda \operatorname{sg}[\bar{H}_t^{(i)}] \right|, \tag{7}$$

with $\lambda \geq 0$ and stop-gradient $sg[\cdot]$. Zeroing low-entropy updates *saves* roughly $p_{lo}|A^{(i)}|$ of mass and *reinvests* it on high-entropy tokens through the additive bonus $\lambda sg[\bar{H}_t^{(i)}]$.

Proposition 1 (Per-batch budget balance). For a batch B, choose

$$\lambda^{\star} \triangleq \kappa \cdot \frac{\sum_{i \in \mathcal{B}} \left| A^{(i)} \right| \cdot \frac{1}{T^{(i)}} \sum_{t \in \mathcal{S}_{\text{b,i}}^{(i,m)}} 1}{\sum_{i \in \mathcal{B}} \frac{1}{T^{(i)}} \sum_{t \in \mathcal{S}_{\text{b,i}}^{(i,m)}} \text{sg}[\bar{H}_{t}^{(i)}]} \quad \text{with } \kappa \in (0, 1].$$

$$(8)$$

Then $\mathbb{E}_{\mathcal{B}}[B_{\mathrm{EG}}^{(i)}] \approx \kappa \cdot \mathbb{E}_{\mathcal{B}}[B_{\mathrm{GRPO}}^{(i)}]$. A detailed derivation and calibration discussion are deferred to Appendix B.1. Setting $\kappa = 1$ yields batch-level budget neutrality in the calibrated upper-bound sense.

Fixed-point neutrality. Because λ^* scales with $\sum_i |A^{(i)}|$, the bonus vanishes at GRPO equilibrium where group-relative advantages cancel. See Appendix B.2 for a formal proof.

Corollary 5.1 (Preserving GRPO stationary points). If $A^{(i)} \equiv 0$ for all i and $\lambda = \lambda^*$ with $\kappa = 1$, then $\lambda^* = 0$ and $\tilde{A}_t^{(i)} \equiv 0$ for all t; EG-GRPO reduces to the KL regularizer and preserves the stationary point.

5.4 ENTROPY-BIASED ADVANTAGE

We modify the broadcasted coefficient at token t of sequence i by

$$\tilde{A}_{t}^{(i)} = M_{t}^{(i)} A^{(i)} + U_{t}^{(i)} \lambda \operatorname{sg}[\bar{H}_{t}^{(i)}], \tag{9}$$

where $M_t^{(i)}$ removes reward-driven updates on the lowest-entropy 20% tokens and $U_t^{(i)}$ adds an entropy bonus on the highest-entropy 50% tokens. The EG-GRPO loss is

$$\mathcal{L}_{\text{EG-GRPO}}(\theta) = -\frac{1}{G} \sum_{i=1}^{G} \frac{1}{T^{(i)}} \sum_{t=1}^{T^{(i)}} \tilde{A}_{t}^{(i)} \log \pi_{\theta} \left(o_{t}^{(i)} \mid c, o_{< t}^{(i)} \right) + \beta D_{\text{KL}} \left(\pi_{\theta} \parallel \pi_{\text{ref}} \right). \tag{10}$$

 β and the reference-policy KL are unchanged; low-entropy tokens are therefore governed solely by KL when $M_t^{(i)}=0$.

Reward-shaping view. Define a token-level pseudo-reward $\tilde{r}_t^{(i)} \triangleq r_{\text{grp}}^{(i)} \cdot M_t^{(i)} + \lambda \operatorname{sg}[\bar{H}_t^{(i)}] \cdot U_t^{(i)}$, where $r_{\text{grp}}^{(i)}$ induces $A^{(i)}$. Then $\mathbb{E}\left[\nabla_{\theta} \log \pi_{\theta}(o_t^{(i)} \mid \cdot) \tilde{r}_t^{(i)}\right]$ is an unbiased policy-gradient estimator for an augmented objective whose baseline component is GRPO.

5.5 WHY EG-GRPO REDUCES UNCERTAINTY AND PRESERVES KNOWLEDGE

(A) Targeted entropy reduction. For small steps, the update at token t is proportional to $\tilde{A}_t^{(i)} \nabla_{\theta} \log \pi_{\theta}(o_t^{(i)} \mid \cdot)$. On high-entropy tokens, $\tilde{A}_t^{(i)} = A^{(i)} + \lambda \operatorname{sg}[\bar{H}_t^{(i)}]$ strengthens positive updates and attenuates negative ones, lowering entropy where it is largest under softmax parameterizations.

(B) Stability on confident tokens. When $M_t^{(i)} = 0$, reward-driven gradients vanish and only KL-to-reference remains, protecting confident regions from drift and preserving learned knowledge.

(C) Proximity to GRPO equilibrium. With $\lambda = \lambda^*$ and $\kappa = 1$, the batch-wise coefficient budget matches GRPO (Appendix B.1), and the bonus disappears at equilibrium (Appendix B.2), reallocating update mass without altering stationary points.

6 EXPERIMENTS

6.1 EXPERIMENTAL SETTINGS

Training Details. Following (Jiang et al., 2025), we train our policy on the same 6,786 text prompts drawn from T2I-CompBench Huang et al. (2023), which contain only textual descriptions without paired images. The prompts are accompanied by structured object–attribute annotations that were automatically extracted using GPT-40 mini in prior work (Jiang et al., 2025). The policy backbone is initialized from Janus-Pro-7B Chen et al. (2025). Optimization uses a learning rate of 1×10^{-6} and a KL coefficient $\beta = 0.01$. For the reward pipeline, we combine HPS (Wu et al., 2023) as the human-preference estimator, GroundingDINO (Liu et al., 2024) as the object detector, and GIT (Wang et al., 2022) as the VQA model. The object–relation module (ORM) is implemented by finetuning LLaVA-OneVision-7B following the procedure of Guo et al. (2025).

Benchmark. To assess the effectiveness of our approach, we rely on two established evaluation suites: T2I-CompBench Huang et al. (2023) and WISE Niu et al. (2025). T2I-CompBench provides 6,000 prompts designed to test compositional generalization. The benchmark covers three broad categories: attribute binding, object relations, and complex compositions, which are further split into six sub-categories, such as color/shape/texture bindings, spatial and non-spatial relations, and multi-object compositions. In contrast, WISE focuses on knowledge-intensive reasoning. It contains 1,000 prompts spanning cultural commonsense, spatial—temporal reasoning, and natural science, requiring the model to infer what specific entity or situation should appear in the image. For WISE, since the corresponding reasoning instructions from prior work (Jiang et al., 2025) were not released, we reimplemented them ourselves and provide the exact templates in the Appendix C for transparency. For both benchmarks, we otherwise follow the official evaluation protocols.

6.2 Main Results

Model	T2I-CompBench		WISE			
	Color	Shape	Texture	Culture	Spatio-temporal	Science
PixArt- α (Chen et al., 2023)	66.90	49.27	64.77	45.00	50.00	46.30
SD-v1.5 (Rombach et al., 2022)	37.58	37.13	41.86	34.00	33.50	26.00
FLUX.1-dev (Labs, 2024)	74.07	57.18	69.22	48.00	59.00	45.00
Emu3 (Wang et al., 2024)	75.44	57.06	71.64	34.00	45.00	37.70
Show-o (Xie et al., 2024)	56.00	41.00	46.00	28.00	45.00	37.30
Janus-Pro-7B (Chen et al., 2025)	63.59	35.28	49.36	30.00	37.00	34.70
T2I-R1* (Jiang et al., 2025)	81.86	57.35	75.40	47.00	55.50	43.67
EG-GRPO (Ours)	84.85	62.61	78.13	48.00	55.00	44.00

Table 1: Comparison of models across **T2I-CompBench** and **WISE**. Spatio-temporal is the average of Time and Space; Science is the average of Biology, Physics, and Chemistry. *Results for T2I-R1 are reproduced under the same experimental settings for fair comparison.

As shown in Table 1, EG-GRPO achieves the strongest results on T2I-CompBench, surpassing all baselines in Color (84.85), Shape (62.61), and Texture (78.13), with particularly notable gains on Shape binding. On WISE, EG-GRPO improves over T2I-R1 in Culture (48.00 vs. 47.00) while maintaining comparable performance in Spatio-temporal (55.00 vs. 55.50) and Science (44.00 vs. 43.67). These consistent improvements demonstrate that entropy-guided updates effectively enhance compositional reasoning and robustness while preserving the stability of knowledge learned by the base model.

6.3 ABLATION STUDY

Table 2 summarizes the effect of applying entropy guidance on different token types. The full EG-GRPO model, which adds entropy bonuses to both textual CoT tokens and image tokens, achieves the best overall performance. Restricting entropy guidance to only CoT tokens (*wl only sem*) or only image tokens (*wl only tok*) leads to weaker results, indicating that both modalities benefit from uncertainty reduction. The baseline without entropy guidance (*wlo All*) performs worst, confirming that the proposed entropy-aware updates are essential for improved compositional generalization.

Model	Color	Shape	Texture
EG-GRPO	84.85	62.61	78.13
w/ only sem w/ only tok w/o All	81.87 84.08 81.86	56.79 61.80 57.35	75.02 77.88 75.40

Table 2: Ablation results of EG-GRPO. We compare the full method with variants that apply entropy guidance only to textual CoT tokens (w/only sem), only to image tokens (w/only tok), or not at all (w/o All).

6.4 Analysis of Entropy

Figure 5 shows the entropy distributions of EG-GRPO and T2I-R1 on textual CoT tokens (left) and image tokens (right). EG-GRPO reduces both the mean and variance of entropy, with a stronger effect on image tokens, indicating that our method concentrates updates on uncertain regions and yields more confident yet stable predictions without sacrificing diversity.

6.5 CASE STUDY

As shown in Figure 6, our method consistently produces high-quality generations across a wide range of prompts. It captures fine-grained attributes such as colors and textures with higher fidelity, preserves coherent spatial layouts in complex scenes, and maintains stability when composing multiple objects. These results confirm that entropyguided optimization enhances both the accuracy and consistency of text-to-image generation.

7 Conclusion

We studied entropy dynamics in text-to-image generation, showing that CoT expands exploration while reinforcement learning contracts it toward stable, high-reward regions. Both the mean and variance of entropy strongly predict image quality, motivating our Entropy-Guided GRPO (EG-GRPO). By protecting low-entropy tokens and focusing updates on high-entropy ones, EG-GRPO balances stability with structured exploration. Experiments on T2I-CompBench and WISE confirm its state-of-the-art performance and reduced instability, underscoring uncertainty control as a key principle for advancing text-to-image generation.

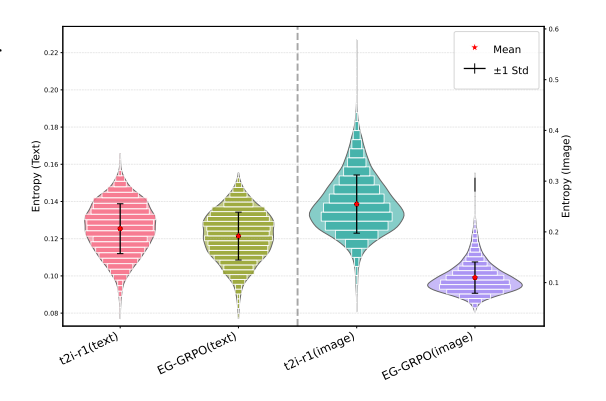


Figure 5: Entropy distributions of EG-GRPO vs. T2I-R1: left for textual CoT tokens, right for image tokens.



Figure 6: Qualitative case study of our method on diverse prompts.

REFERENCES

- Junsong Chen, Jincheng Yu, Chongjian Ge, Lewei Yao, Enze Xie, Yue Wu, Zhongdao Wang, James Kwok, Ping Luo, Huchuan Lu, et al. Pixart-alpha: Fast training of diffusion transformer for photorealistic text-to-image synthesis. arXiv preprint arXiv:2310.00426, 2023.
- Xiaokang Chen, Zhiyu Wu, Xingchao Liu, Zizheng Pan, Wen Liu, Zhenda Xie, Xingkai Yu, and Chong Ruan. Janus-pro: Unified multimodal understanding and generation with data and model scaling. *arXiv preprint arXiv:2501.17811*, 2025.
- Lijie Fan, Tianhong Li, Siyang Qin, Yuanzhen Li, Chen Sun, Michael Rubinstein, Deqing Sun, Kaiming He, and Yonglong Tian. Fluid: Scaling autoregressive text-to-image generative models with continuous tokens. *arXiv preprint arXiv:2410.13863*, 2024.
- Ying Fan, Olivia Watkins, Yuqing Du, Hao Liu, Moonkyung Ryu, Craig Boutilier, Pieter Abbeel, Mohammad Ghavamzadeh, Kangwook Lee, and Kimin Lee. Dpok: Reinforcement learning for fine-tuning text-to-image diffusion models. *Advances in Neural Information Processing Systems*, 36:79858–79885, 2023.
- Zhida Feng, Zhenyu Zhang, Xintong Yu, Yewei Fang, Lanxin Li, Xuyi Chen, Yuxiang Lu, Jiaxiang Liu, Weichong Yin, Shikun Feng, et al. Ernie-vilg 2.0: Improving text-to-image diffusion model with knowledge-enhanced mixture-of-denoising-experts. In *Proceedings of the IEEE/CVF Conference on Computer Vision and Pattern Recognition*, pp. 10135–10145, 2023.
- Shuyang Gu, Dong Chen, Jianmin Bao, Fang Wen, Bo Zhang, Dongdong Chen, Lu Yuan, and Baining Guo. Vector quantized diffusion model for text-to-image synthesis. In *Proceedings of the IEEE/CVF conference on computer vision and pattern recognition*, pp. 10696–10706, 2022.
- Ziyu Guo, Renrui Zhang, Chengzhuo Tong, Zhizheng Zhao, Rui Huang, Haoquan Zhang, Manyuan Zhang, Jiaming Liu, Shanghang Zhang, Peng Gao, et al. Can we generate images with cot? let's verify and reinforce image generation step by step. *arXiv* preprint arXiv:2501.13926, 2025.
- Kaiyi Huang, Kaiyue Sun, Enze Xie, Zhenguo Li, and Xihui Liu. T2i-compbench: A comprehensive benchmark for open-world compositional text-to-image generation. *Advances in Neural Information Processing Systems*, 36:78723–78747, 2023.
- Dongzhi Jiang, Ziyu Guo, Renrui Zhang, Zhuofan Zong, Hao Li, Le Zhuo, Shilin Yan, Pheng-Ann Heng, and Hongsheng Li. T2i-r1: Reinforcing image generation with collaborative semantic-level and token-level cot. *arXiv preprint arXiv:2505.00703*, 2025.
- Black Forest Labs. Flux. https://github.com/black-forest-labs/flux, 2024.
- Wei Li, Xue Xu, Xinyan Xiao, Jiachen Liu, Hu Yang, Guohao Li, Zhanpeng Wang, Zhifan Feng, Qiaoqiao She, Yajuan Lyu, et al. Upainting: Unified text-to-image diffusion generation with cross-modal guidance. *arXiv preprint arXiv:2210.16031*, 2022.
- Yaqi Li, Peng Chen, Mingyang Han, Bu Pi, Haoxiang Shi, Runzhou Zhao, Yang Yao, Xuan Zhang, and Jun Song. Visual-cog: Stage-aware reinforcement learning with chain of guidance for text-to-image generation. *arXiv* preprint arXiv:2508.18032, 2025.
- Jiaqi Liao, Zhengyuan Yang, Linjie Li, Dianqi Li, Kevin Lin, Yu Cheng, and Lijuan Wang. Imagegen-cot: Enhancing text-to-image in-context learning with chain-of-thought reasoning. arXiv preprint arXiv:2503.19312, 2025.
- Shilong Liu, Zhaoyang Zeng, Tianhe Ren, Feng Li, Hao Zhang, Jie Yang, Qing Jiang, Chunyuan Li, Jianwei Yang, Hang Su, et al. Grounding dino: Marrying dino with grounded pre-training for open-set object detection. In *European conference on computer vision*, pp. 38–55. Springer, 2024.
 - Xiaoxiao Ma, Mohan Zhou, Tao Liang, Yalong Bai, Tiejun Zhao, Huaian Chen, and Yi Jin. Star: Scale-wise text-to-image generation via auto-regressive representations. *arXiv e-prints*, pp. arXiv–2406, 2024.

- Yanting Miao, William Loh, Suraj Kothawade, Pascal Poupart, Abdullah Rashwan, and Yeqing Li. Subject-driven text-to-image generation via preference-based reinforcement learning. *Advances in Neural Information Processing Systems*, 37:123563–123591, 2024.
- Yuwei Niu, Munan Ning, Mengren Zheng, Weiyang Jin, Bin Lin, Peng Jin, Jiaqi Liao, Chaoran Feng, Kunpeng Ning, Bin Zhu, et al. Wise: A world knowledge-informed semantic evaluation for text-to-image generation. *arXiv preprint arXiv:2503.07265*, 2025.
- Robin Rombach, Andreas Blattmann, Dominik Lorenz, Patrick Esser, and Björn Ommer. High-resolution image synthesis with latent diffusion models. In *Proceedings of the IEEE/CVF conference on computer vision and pattern recognition*, pp. 10684–10695, 2022.
- NextStep Team, Chunrui Han, Guopeng Li, Jingwei Wu, Quan Sun, Yan Cai, Yuang Peng, Zheng Ge, Deyu Zhou, Haomiao Tang, et al. Nextstep-1: Toward autoregressive image generation with continuous tokens at scale. *arXiv* preprint arXiv:2508.10711, 2025.
- Chengzhuo Tong, Ziyu Guo, Renrui Zhang, Wenyu Shan, Xinyu Wei, Zhenghao Xing, Hongsheng Li, and Pheng-Ann Heng. Delving into rl for image generation with cot: A study on dpo vs. grpo. *arXiv preprint arXiv:2505.17017*, 2025.
- Michael Tschannen, André Susano Pinto, and Alexander Kolesnikov. Jetformer: An autoregressive generative model of raw images and text. *arXiv preprint arXiv:2411.19722*, 2024.
- Jianfeng Wang, Zhengyuan Yang, Xiaowei Hu, Linjie Li, Kevin Lin, Zhe Gan, Zicheng Liu, Ce Liu, and Lijuan Wang. Git: A generative image-to-text transformer for vision and language. *arXiv* preprint arXiv:2205.14100, 2022.
- Linqing Wang, Ximing Xing, Yiji Cheng, Zhiyuan Zhao, Jiale Tao, Qixun Wang, Ruihuang Li, Xin Li, Mingrui Wu, Xinchi Deng, et al. Promptenhancer: A simple approach to enhance text-to-image models via chain-of-thought prompt rewriting. *arXiv preprint arXiv:2509.04545*, 2025a.
- Shenzhi Wang, Le Yu, Chang Gao, Chujie Zheng, Shixuan Liu, Rui Lu, Kai Dang, Xionghui Chen, Jianxin Yang, Zhenru Zhang, et al. Beyond the 80/20 rule: High-entropy minority tokens drive effective reinforcement learning for llm reasoning. *arXiv preprint arXiv:2506.01939*, 2025b.
- Xinlong Wang, Xiaosong Zhang, Zhengxiong Luo, Quan Sun, Yufeng Cui, Jinsheng Wang, Fan Zhang, Yueze Wang, Zhen Li, Qiying Yu, et al. Emu3: Next-token prediction is all you need. *arXiv preprint arXiv:2409.18869*, 2024.
- Jason Wei, Xuezhi Wang, Dale Schuurmans, Maarten Bosma, Fei Xia, Ed Chi, Quoc V Le, Denny Zhou, et al. Chain-of-thought prompting elicits reasoning in large language models. Advances in neural information processing systems, 35:24824–24837, 2022.
- Ren-Di Wu, Yu-Yen Lin, and Huei-Fang Yang. Training-free zero-shot composed image retrieval via weighted modality fusion and similarity. In *International Conference on Technologies and Applications of Artificial Intelligence*, pp. 77–90. Springer, 2024.
- Xiaoshi Wu, Yiming Hao, Keqiang Sun, Yixiong Chen, Feng Zhu, Rui Zhao, and Hongsheng Li. Human preference score v2: A solid benchmark for evaluating human preferences of text-to-image synthesis. *arXiv preprint arXiv:2306.09341*, 2023.
- Jinheng Xie, Weijia Mao, Zechen Bai, David Junhao Zhang, Weihao Wang, Kevin Qinghong Lin, Yuchao Gu, Zhijie Chen, Zhenheng Yang, and Mike Zheng Shou. Show-o: One single transformer to unify multimodal understanding and generation. *arXiv* preprint arXiv:2408.12528, 2024.
- Ling Yang, Zhaochen Yu, Chenlin Meng, Minkai Xu, Stefano Ermon, and Bin Cui. Mastering text-to-image diffusion: Recaptioning, planning, and generating with multimodal llms. In *Forty-first International Conference on Machine Learning*, 2024.
- Jiahui Yu, Yuanzhong Xu, Jing Yu Koh, Thang Luong, Gunjan Baid, Zirui Wang, Vijay Vasudevan, Alexander Ku, Yinfei Yang, Burcu Karagol Ayan, et al. Scaling autoregressive models for contentrich text-to-image generation. *arXiv* preprint arXiv:2206.10789, 2(3):5, 2022.

Renrui Zhang, Chengzhuo Tong, Zhizheng Zhao, Ziyu Guo, Haoquan Zhang, Manyuan Zhang, Jiaming Liu, Peng Gao, and Hongsheng Li. Let's verify and reinforce image generation step by step. In *Proceedings of the Computer Vision and Pattern Recognition Conference*, pp. 28662–28672, 2025a.

Yu Zhang, Yunqi Li, Yifan Yang, Rui Wang, Yuqing Yang, Dai Qi, Jianmin Bao, Dongdong Chen, Chong Luo, and Lili Qiu. Reasongen-r1: Cot for autoregressive image generation models through sft and rl. *arXiv preprint arXiv:2505.24875*, 2025b.

A THE USE OF LARGE LANGUAGE MODELS

In this work, we employed GPT-5 to assist with the polishing of English text. The model was used primarily for improving readability, clarity, and fluency of the written content, ensuring that the final manuscript meets high academic standards.

B PROOFS AND DERIVATIONS FOR EG-GRPO

B.1 DETAILED PROOF OF PROPOSITION 1 (PER-BATCH BUDGET BALANCE)

Setup and notation. For sequence i, write $a^{(i)} \triangleq |A^{(i)}| \geq 0$, $s^{(i)} \triangleq \operatorname{sign}(A^{(i)}) \in \{\pm 1\}$, and $h_t^{(i)} \triangleq \bar{H}_t^{(i)} \in [0,1]$. With the low/mid/high partitions from Section 5.3, EG-GRPO's per-sequence budget can be written as

$$B_{\rm EG}^{(i)} = (1 - p_{\rm lo}) a^{(i)} + \frac{1}{T^{(i)}} \sum_{t \in \mathcal{S}_{c}^{(i,m)}} \left(\left| s^{(i)} a^{(i)} + \lambda h_{t}^{(i)} \right| - a^{(i)} \right). \tag{11}$$

Lemma 1 (Symmetric sign averaging). For any $a \ge 0$ and $b \ge 0$,

$$\frac{1}{2}\Big(|a+b|+|-a+b|\Big)=\max(a,b).$$

Proof. If $b \ge a$, then |a+b| = a+b and |-a+b| = b-a, so the average is b. If b < a, then |a+b| = a+b and |-a+b| = a-b, so the average is a.

Exact decomposition. Taking expectation over $s^{(i)}$ (assumed approximately symmetric due to group-normalization), Lemma 1 yields

$$\mathbb{E}_{s^{(i)}}[|s^{(i)}a^{(i)} + \lambda h_t^{(i)}|] = \max(a^{(i)}, \lambda h_t^{(i)}). \tag{12}$$

Plugging into equation 11 and using $(x-a)_+ \triangleq \max(0, x-a)$,

$$\mathbb{E}_{s^{(i)}}[B_{\text{EG}}^{(i)}] = (1 - p_{\text{lo}}) a^{(i)} + \underbrace{\frac{1}{T^{(i)}} \sum_{t \in \mathcal{S}_{\text{hi}}^{(i,m)}} (\lambda h_t^{(i)} - a^{(i)})_+}_{\delta^{(i)}(\lambda)}.$$
(13)

Averaging over the batch \mathcal{B} gives

$$\mathbb{E}_{\mathcal{B}}[B_{\text{EG}}^{(i)}] = (1 - p_{\text{lo}}) \,\mathbb{E}_{\mathcal{B}}[a^{(i)}] + \mathbb{E}_{\mathcal{B}}[\delta^{(i)}(\lambda)]. \tag{14}$$

Here $\delta^{(i)}(\lambda)$ is nondecreasing in λ and equals zero at $\lambda = 0$.

Target equation for exact κ -scaling. If one desires $\mathbb{E}_{\mathcal{B}}[B_{\mathrm{EG}}^{(i)}] = \kappa \mathbb{E}_{\mathcal{B}}[a^{(i)}]$, then equation 14 is equivalent to

$$\sum_{i \in \mathcal{B}} \frac{1}{T^{(i)}} \sum_{t \in \mathcal{S}_{\text{l.}}^{(i,m)}} (\lambda h_t^{(i)} - a^{(i)})_+ = (\kappa - 1 + p_{\text{lo}}) \sum_{i \in \mathcal{B}} a^{(i)}.$$
 (15)

The left-hand side is continuous, nondecreasing in λ , hence admits a (numerically) unique solution for any $\kappa \in (0, 1]$.

Closed-form calibration (upper-bound match). For an implementable closed form, use $(x - a)_+ \le x$ with $x = \lambda h_{\star}^{(i)}$:

$$\delta^{(i)}(\lambda) \leq \lambda \cdot \underbrace{\frac{1}{T^{(i)}} \sum_{t \in \mathcal{S}_{\mathrm{hi}}^{(i,m)}} h_t^{(i)}}_{H_{\mathrm{hi}}^{(i)}}.$$

Substituting this into equation 14 yields the upper bound

$$\mathbb{E}_{\mathcal{B}}[B_{\mathrm{EG}}^{(i)}] \le (1 - p_{\mathrm{lo}}) \,\mathbb{E}_{\mathcal{B}}[a^{(i)}] + \lambda \,\mathbb{E}_{\mathcal{B}}[H_{\mathrm{hi}}^{(i)}]. \tag{16}$$

Matching the *upper bound* to $\kappa \mathbb{E}_{\mathcal{B}}[a^{(i)}]$ leads to the batch-calibrated choice

$$\lambda^{\star} \triangleq \kappa \cdot \frac{\sum_{i \in \mathcal{B}} a^{(i)} \cdot \frac{1}{T^{(i)}} \sum_{t \in \mathcal{S}_{lo}^{(i,m)}} 1}{\sum_{i \in \mathcal{B}} \frac{1}{T^{(i)}} \sum_{t \in \mathcal{S}_{lo}^{(i,m)}} h_t^{(i)}} = \kappa \cdot \frac{\sum_{i \in \mathcal{B}} |A^{(i)}| \cdot \frac{|\mathcal{S}_{lo}^{(i,m)}|}{T^{(i)}}}{\sum_{i \in \mathcal{B}} \frac{1}{T^{(i)}} \sum_{t \in \mathcal{S}_{lo}^{(i,m)}} \operatorname{sg}[\bar{H}_t^{(i)}]},$$
(17)

which is exactly equation 8. This calibration equates "saved" low-entropy budget with "reinvested" high-entropy mass in an upper-bound sense; see Remarks below.

Remarks on calibration accuracy. (i) Define the nonnegative discrepancy

$$\varepsilon^{(i)}(\lambda) \triangleq \lambda H_{\mathrm{hi}}^{(i)} - \delta^{(i)}(\lambda) = \frac{1}{T^{(i)}} \sum_{t \in \mathcal{S}_{\mathrm{hi}}^{(i,m)}} \min(\lambda h_t^{(i)}, a^{(i)}).$$

It vanishes as $\lambda h_t^{(i)} \gg a^{(i)}$ for most high-entropy tokens, and is statistically damped by batch averaging. (ii) For exact κ -scaling, one may solve equation 15 via a 1D root finder; we keep equation 8 for simplicity and stability. (iii) With $\kappa=1$, equation 8 delivers batch-level budget neutrality in the calibrated upper-bound sense; empirically it closely tracks neutrality while avoiding per-step root solving.

Conclusion. Combining equation 14–equation 16 with the calibration above yields $\mathbb{E}_{\mathcal{B}}[B_{\mathrm{EG}}^{(i)}] \approx \kappa \mathbb{E}_{\mathcal{B}}[B_{\mathrm{GRPO}}^{(i)}]$, as stated in Proposition 1.

B.2 PROOF OF COROLLARY 5.1 (FIXED-POINT NEUTRALITY)

Suppose $A^{(i)} \equiv 0$ for all i in a batch. Then $a^{(i)} = 0$, and the numerator of equation 8 vanishes, yielding $\lambda^{\star} = 0$ for any $\kappa \in (0,1]$. By equation 9, $\tilde{A}_t^{(i)} \equiv 0$ for all tokens t, so the loss equation 10 reduces to the reference-policy KL term. Hence any GRPO stationary point remains stationary under EG-GRPO, proving the corollary.

B.3 OPTIONAL EXACT PER-BATCH SCALING (IMPLEMENTATION NOTE)

If precise κ -scaling is required, solve the monotone equation equation 15 for λ by bisection or Newton's method. This guarantees $\mathbb{E}_{\mathcal{B}}[B_{\mathrm{EG}}^{(i)}] = \kappa \, \mathbb{E}_{\mathcal{B}}[B_{\mathrm{GRPO}}^{(i)}]$ exactly per batch, at the cost of a 1D search.

C INSTRUCTION FOR WISE

WISE Instruction

 You are asked to write a concise text description to guide the generation of an image based on this prompt: "{}". Provide a brief, precise visualization of all elements in the prompt. Your description should:

- 1. Include every object mentioned.
- 2. Specify visual attributes (color, number, shape, texture) if given.
- 3. Clarify spatial or relational positioning if specified.
- 4. Be concise (\leq 50 words) but include the most common features and states inferred from real-world knowledge.
- 5. Apply real-world knowledge (cultural, religious, temporal, spatial, biological, physical, or chemical reasoning) and select only the single most relevant aspect that naturally enhances the original prompt to infer context (e.g., season, appearance, identity, cultural usage, or natural state) and reflect it in the objects. Use direct, widely accepted interpretations; include cultural or religious meanings only when they are common real-world associations. Avoid abstract or purely metaphorical interpretations.
- 6. Emphasize the current state of each object individually, as inferred from its environment or context. Reason separately for each object, considering temporal, cultural, or physical factors, and prioritize states logically implied by the prompt.
- 7. If multiple objects are present, reason from each object's inherent physical or chemical properties and their interactions with the environment and with all other objects. Ensure that the inferred state, behavior, and interaction of every single object is logically correct and consistent with real-world rules, and clearly describe all differences and interactions relative to each other.
- 8. Ensure realism and aesthetic quality: all objects and interactions must follow real-world rules and appear visually consistent and appealing.
- 9. Do not omit objects explicitly mentioned, or add ones not specified or logically inferred.
- 10. Always preserve and emphasize the original objects and scene as the primary focus.
- 11. Always output a complete natural language description, never an image or symbolic shorthand.

#